Cavitation instabilities in hydraulic machines

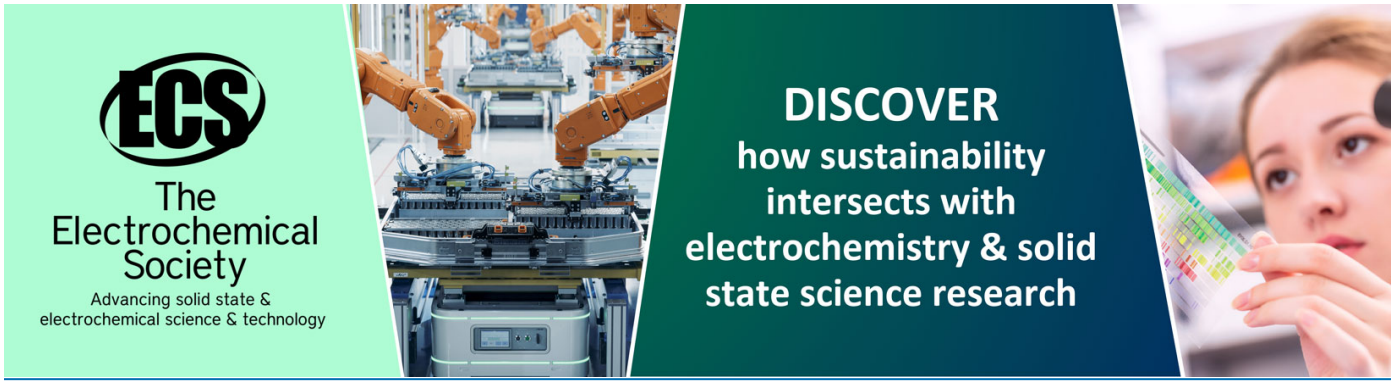

Cavitation instabilities in hydraulic machines

Y Tsujimoto

Engineering Science, Osaka University., Osaka 560-8531, Japan

E-mail: tujimoto@me.es.osaka-u.ac.jp

Abstract. Cavitation instabilities in hydraulic machines, hydro turbines and turbopump inducers, are reviewed focusing on the cause of instabilities. One-dimensional model of hydro turbine system shows that the overload surge is caused by the diffuser effect of the draft tube. Experiments show that this effect also causes the surge mode oscillations at part load. One dimensional model of a cavitating turbopump inducer shows that the mass flow gain factor, representing the cavity volume increase caused by the incidence angle increase is the cause of cavitation surge and rotating cavitation. Two dimensional model of a cavitating turbopump inducer shows that various modes of cavitation instabilities start to occur when the cavity length becomes about 65% of the blade spacing. This is caused by the interaction of the local flow near the cavity trailing edge with the leading edge of the next blade. It was shown by a 3D CFD that this is true also for real cases with tip cavitation. In all cases, it was shown that cavitation instabilities are caused by the fundamental characteristics of cavities that the cavity volume increases with the decrease of ambient pressure or the increase of the incidence angle.

1. Introduction

Surge and rotating stall are well known as instabilities in turbomachinery. These occur both in pneumatic and hydraulic machines caused by the positive slope of the performance curve associated with stall. If the flow rate is increased, the pressure rise increases following the positive slope and the flow rate is increased further driven by the pressure rise increase. For the surge to occur, some compliance should exist in the pipeline to constitute a vibration system. In pneumatic machines with a high tip Mach number, some part of the pipeline can serve as the compliance and an organ pipe type surge can occur. In hydraulic machines, if cavitation occurs, it serves as a compliant element and a surge can occur even without an explicit compliant element in the system.

Cavitation instabilities can be different from those in non-cavitating systems since cavitation instabilities can occur even at design flow rate where the slope of performance curve is negative. The present paper treats cavitation instabilities focusing on the cause of instabilities.

2. Cavitation instabilities in hydraulic turbine system

Figure 1 shows the spectrum of pressure fluctuation at the outlet of a Francis turbine[1]. The horizontal axis is the frequency normalized with the rotational frequency of the runner plotted for various flow rates normalized with the design flow rate. Hydraulic turbines are designed so that the flow exits the runner without swirl at design flow rate. Figure 2 shows the velocity triangle at the runner exit. The runner is rotating with the velocity U_2 and it is assumed that the relative velocity w_2 is tangential to the blade surface which has the outlet blade angle of β_2. S is the cross-sectional area of the runner exit. At the design flow rate of $Q_{sf} = Q_{nDref}$, the absolute velocity of c_{sf} is without swirl while it has a tangential component in the same/opposite direction as/to the runner rotation below (Q_a)/above (Q_b)

design flow rate.

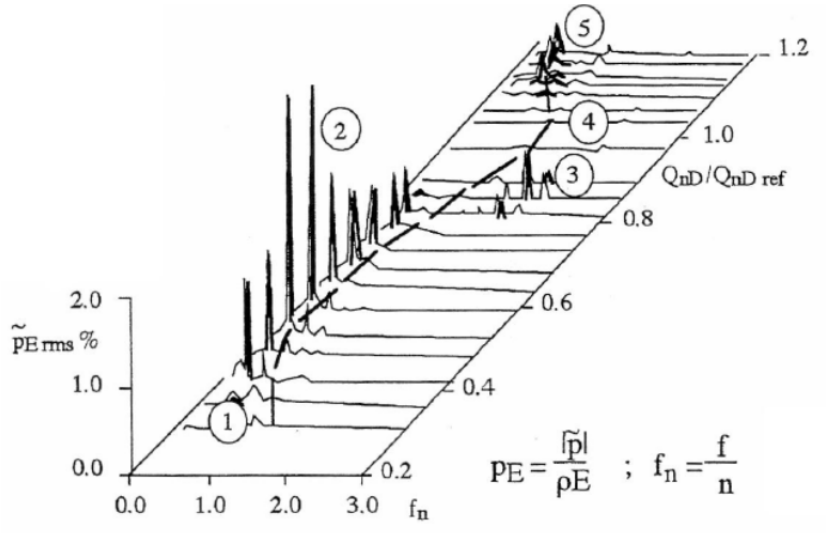

Figure 1. Pressure fluctuation at the runner exit[1].

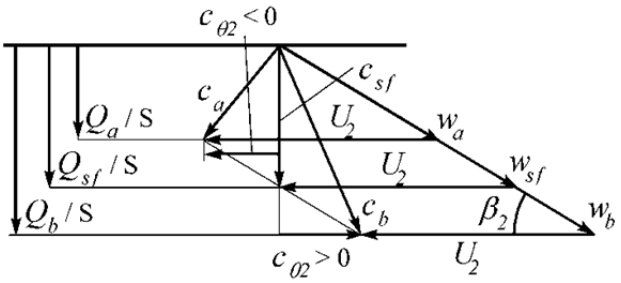

Figure 2. Velocity triangle at the runner exit.

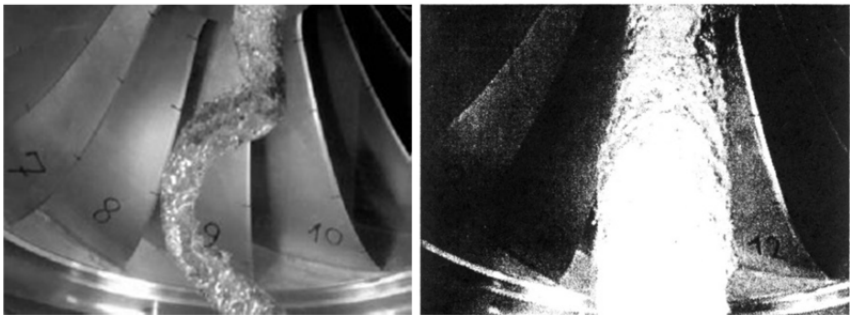

(a) $Q_a / Q_{sf} = Q_{nD} / Q_{nD\,ref} < 1$ (b) $Q_b / Q_{sf} = Q_{nD} / Q_{nD\,ref} > 1$

Figure 3. Cavitation at runner exit.

Figure 3 shows the cavitation at the runner exit. At part load with $Q_a / Q_{sf} = Q_{nD} / Q_{nD\,ref} < 1$, a cork screw vortex rope appears around the backflow region at the center of the draft tube and rotates in the same direction as the runner. The component ② in Fig.1 is caused by the rotation of the vortex rope structure and the amplitude becomes the maximum when the frequency agrees the natural frequency of the system associated with the compliance due to cavitation. This has been extensively studied by Nishi[2] and Doerfler[3]. On the other hand, the component ⑤ in Fig.1 appears at overload $Q_b / Q_{sf} = Q_{nD} / Q_{nDref} > 1$. At overload, the absolute flow angle from axial direction is small as shown in Fig.2 and a straight cavitation appears as shown in Fig.3. In certain cases the volume of cavitation

fluctuates extensively and stable operation is hindered. This is called overload surge.

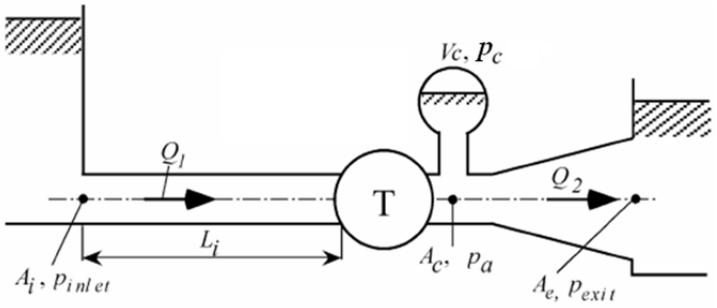

Figure 4. Hydraulic turbine system for stability analysis.

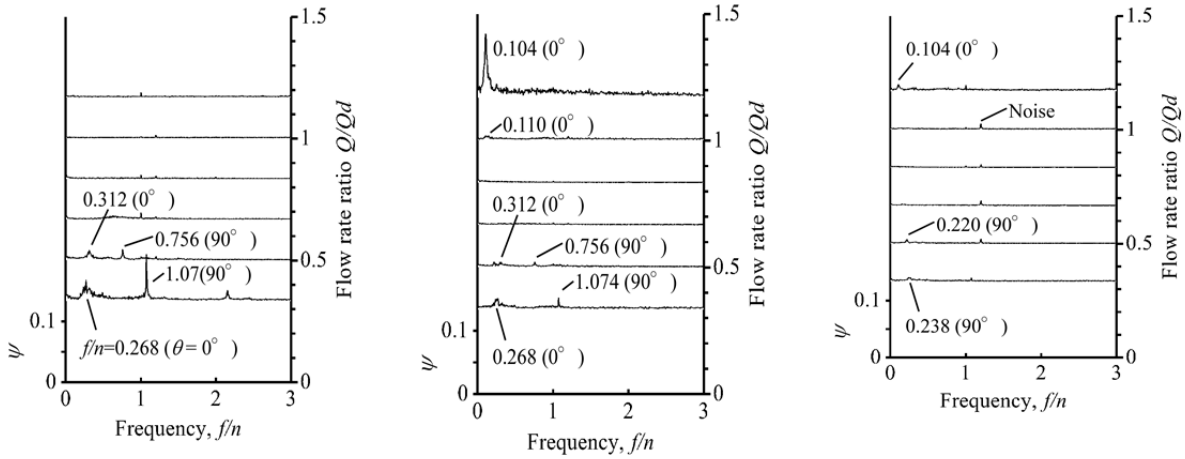

(a) *p*1 (b) *p*2 (c) *p*3

Figure 5. Pressure fluctuation in draft tube, *p1*:near inlet,*p2*:near center, *p3*near exit.

In order to clarify the cause of over-load surge, a stability analysis[3]-[6] has been made on a simplified system as shown in Fig.4. The ambient pressure p_a at the exit of the runner T can be represented as a function of the downstream flow rate Q_2 obtained from unsteady Bernoulli's equation considering the pressure loss. In order to minimize the kinetic energy at the exit, a diffuser called draft tube is placed downstream of the runner. The ambient pressure p_a at the exit of the runner is decreased when the downstream flow rate Q_2 is increased, since the pressure recovery in the draft tube is increased. Then the cavity volume at the runner exit or draft tube inlet is increased and the downstream flow rate Q_2 is increased by the amount of the increasing rate of the cavity volume, if the upstream flow rate Q_1 is kept constant. This effect of pressure recovery in the draft tube makes the hydraulic system with draft tube unstable at all flow rates.

The cavity appears at the core of vortex as shown in Fig.3. The pressure p_c at the vortex core is lower than the ambient pressure p_a caused by the centrifugal force on the swirling flow. We consider the case when the upstream flow rate Q_1 is slightly increased at a smaller flow rate Q_a. Then the velocity triangle in Fig.2 shows that the swirl velocity will decrease and the core pressure p_c increase resulting in the decrease of the cavity volume. Then, the upstream flow Q_1 will increase further to fill up the space of decreased cavity if the downstream flow rate is kept constant. At larger flow rate of Q_b, opposite results are obtained since the swirl velocity will be increased if the flow rate is increased. Thus, the swirl effect destabilizes the system at lower flow rate than the swirl free flow rate and stabilizes at higher flow rate.

In the above discussions, either one of the upstream or downstream flow rate is assumed to be kept constant. However, a stability analysis without the assumption shows that the same result is obtained. Both diffuser and swirl effects are destabilizing at smaller flow rate but the destabilizing effects of

diffuser cancels with the stabilizing effects of swirl at higher flow rate. This shows that the simplified 1-d model cannot completely explain the overload surge shown as ⑤ of Fig.1. However, recent experimental study and CFD[7] shows that the upstream flow rate fluctuation is small and that the surge mode shown by θ =0° exists independently on the swirl mode shown by θ =90° in Fig.5. This shows that the diffuser effect of draft tube is the cause the surge at both smaller and larger than the swirl free flow rate.

3. Instabilities in pumps:1-D stability analysis

In liquid propellant rockets, turbopumps are used to feed the propellants from the low pressure tank to the high pressure combustion chamber and cavitation generally appears at the pump inlet. Since the head is decreased significantly when the cavitation appears in the main impeller, an axial flow pump called "inducer" is used upstream of the main pump. The inducer is designed to have positive incidence at the inlet so that the cavitation appears only on the suction surface of the blades.

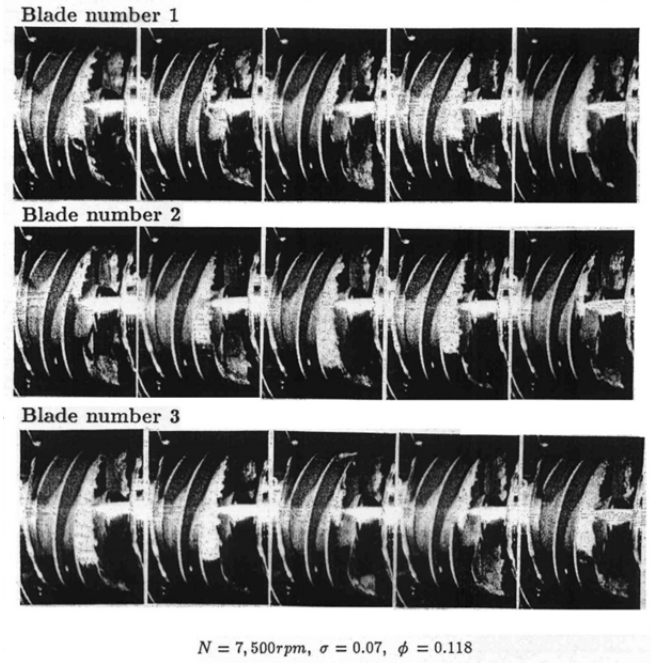

Figure 6. Rotating cavitation.

Figure 6 shows the pictures of cavitation in a 3-bladed inducer. The flow is from right to left and the blades come to the front in the order of Blade 1, 2, and 3. The pictures were taken when they come to the front while the inducer makes 5 turns. White triangular cavities are seen at the tip. During the first turn shown at the left the cavities on Blade 1,3 are larger and the cavity on Blade 2 is small. If we focus on the small cavity, it moves on Blade 2→1→3→2 in the direction of the inducer rotation while the inducer makes 4 turns. This shows that the propagation velocity ratio＝V_p/U_T＝ rotational speed of cavity/rotational speed of inducer＝(4+1)/4=1.25 >1, showing that the cavitation is rotating faster than the inducer. This is called rotating cavitation. This is somewhat similar to rotating stall observed in axial compressors but differs from it on the following aspects. Rotating stalls occur at a small flow rate where the performance curve has a positive slope caused by blade stall. However, rotating cavitation can occur even at design flow rate and higher cavitation number where the head is not decreased by the cavity. The stalled region of rotating stall rotates slower than the impeller but the cavitating region of rotating cavitation rotates faster than the impeller as stated above. This difference suggests the difference of the cause and mechanism of the instabilities. Similar difference can be observed between the surge in compressors and the cavitation surge in pumps. The surge occurs at smaller flow rate with positive slope of the performance curve but cavitation surge can occur even at the design flow rate

without the head decrease caused by stall nor cavitation. This is the same as the relation between rotating stall and rotating cavitation.

In order to clarify the mechanisms of surge, rotating stall, cavitation surge, and rotating cavitation, a 1-D stability analysis was made[9]. Since cavitation surge and rotating cavitation occur under the condition where the head is not decreased by cavitation, the effect of cavitation is taken into account only in the continuity equation using the mass flow gain factor $M=\partial(Vc/h^2)/\partial\alpha$ representing the increase of the cavity volume Vc caused by the increase of the increase of the incidence angle α, and the cavitation compliance $K=-\partial(Vc/h^2)/\partial\sigma$ showing the decrease of the cavity volume caused by the increase of the inlet cavitation number σ. The results are shown in Fig.7.

Instability	Onset condition	Frequency
Surge	$\frac{\partial\psi_{ts}}{\partial\phi} > \frac{1+(1/\cos\beta^*)(l/L)}{B^2\phi R}$	$n=\frac{1}{2\pi}\frac{1}{\sqrt{\rho CL}}\sqrt{\frac{1+(1/R)\left[L_u+\left(1/\cos^2\beta_2^*\right)\right]}{[1+(1/\cos\beta^*)l/s]}}$
Rotating stall	$\frac{\partial\psi_{ts}}{\partial\phi}>0$	$\frac{V_p}{U_T}=1-\frac{2\zeta_s[1-(\phi/\phi^*)]}{1+(2\pi/\cos\beta_1)l/s]}<1$
Cavitation surge	$M>2(1+\sigma)\phi K$	$n=\frac{U_r}{2\pi}\frac{1}{\sin\bar{\beta}_1}\frac{1}{\sqrt{2KLh}}$
Rotating cavitation	$M>2(1+\sigma)\phi K$	$V_p/U_T>1, \quad V_p/U_T<0$

Figure 7. Results of 1-D stability analysis.

Both surge and rotating stall occur when the slope of the performance curve $\partial\psi_{ts}/\partial\sigma$ becomes positive due to stall, while cavitation surge and rotating cavitation occur when the mass flow gain factor becomes positive. When the performance curve has positive slope, the head is increased when the flow rate is increased. Then, the flow rate is increased further being accelerated by the increased head. This is the cause of surge and rotating stall. When the mass flow gain factor is positive, the cavity volume is decreased when the flow rate is increased since the incidence angle is decreased. Then the inlet flow is increased further to fill up the space of collapsing cavity. This is the cause of cavitation surge and rotating cavitation. In the expression of the frequency of surge, $1/2\pi\sqrt{\rho CL}$ is the frequency of Helmholtz resonator with the inlet pipe length L and the compliance C of the tank and the frequency is fixed to the natural frequency of the system. On the other hand, the frequency of cavitation surge is proportional to the tip speed U_T of the rotor and hence the rotational speed. The propagation velocity ratio V_p/U_T of rotating stall is less than one while that of rotating cavitation is either larger than 1 or negative. As mentioned before, the propagation ratio of rotating cavitation is generally larger than 1. However, it was found by experiments that there are certain cases when it becomes negative.

4. Instabilities of pumping system: Two-dimensional stability analysis

The one dimensional analysis mentioned in the last section is convenient for the explanation of the mechanism of instabilities. However, the values of cavitation compliance and mass flow gain factor are difficult to measure and the relation of those factors with the flow detail has not been made clear. To obtain better understanding, a 2-dimensional stability analysis has been made[10],[11]. The flow is represented by the vortex distribution$\gamma_{1,2}$ on the blade surface and the source distribution q on the cavitating part. Since the flow is unsteady, a free vortex γ_t is shed from the blade trailing edge to satisfy unsteady Kutta's condition. The total pressure is specified at the inlet AB to set the pressure level and the absolute flow is assumed to be normal to AB. The values of unknowns $\gamma_{1,2}$ and q are determined based on the boundary conditions that the normal velocity on the wetted surface is zero and that the pressure on the cavity surface equals to the vapor pressure. The values of $\gamma_{1,2}$ and q at discrete points are considered to be unknowns and are separated to steady and unsteady components

assuming that flow disturbances are small. Then, the boundary conditions for the steady components can be expressed as a system of inhomogeneous linear equations:

$$\left[A_{ij}(l_s)\right]\begin{pmatrix}\gamma_j / U\alpha \\ q_j / U\alpha \\ \sigma / 2\alpha\end{pmatrix} = \left(b_i\right) \tag{1}$$

The elements of the coefficient matrix A_{ij} are functions of assumed steady cavity length l_s . Then, Eq.(1) shows that l_s is a function of $\sigma/2\alpha$ where $\sigma = (p_{inlet} - p_v)/(\rho U^2/2)$ is the cavitation number and α is the incidence angle. The unsteady components satisfies the following homogeneous linear equations:

$$\left[B_{ij}(l_s,\omega)\right]\begin{pmatrix}\tilde{\gamma}_j \\ \tilde{q}_j \\ \tilde{l}_s\end{pmatrix} = \left(0\right) \tag{2}$$

If there are forced excitations such as blade vibration or flow rate fluctuation, they appear on the right hand side of Eq.(2) which is zero for the free vibration considered here. The elements of coefficient matrix B_{ij} are functions of steady cavity length l_s and the complex frequency $\omega = \omega_R + j\omega_I$ where ω_R is the frequency and ω_I is the damping rate. In order to have a non-trivial solution, the determinant of B_{ij} should be zero. From this relation we can determine the complex frequency $\omega = \omega_R + j\omega_I$ as a function of steady cavity length l_s. This shows that **the cavitation instabilities of hydrofoils and cascades are generally determined from the steady cavity length l_s and hence the value of $\sigma/2\alpha$**. This is the most important result of the analysis and explains most of experimental results.

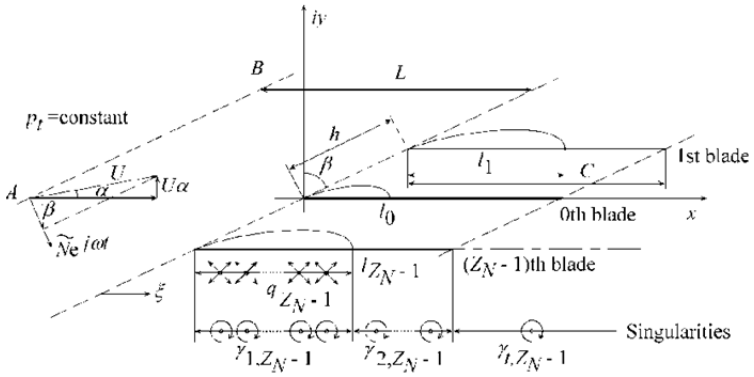

Figure 8. Geometry of two-dimensional stability analysis.

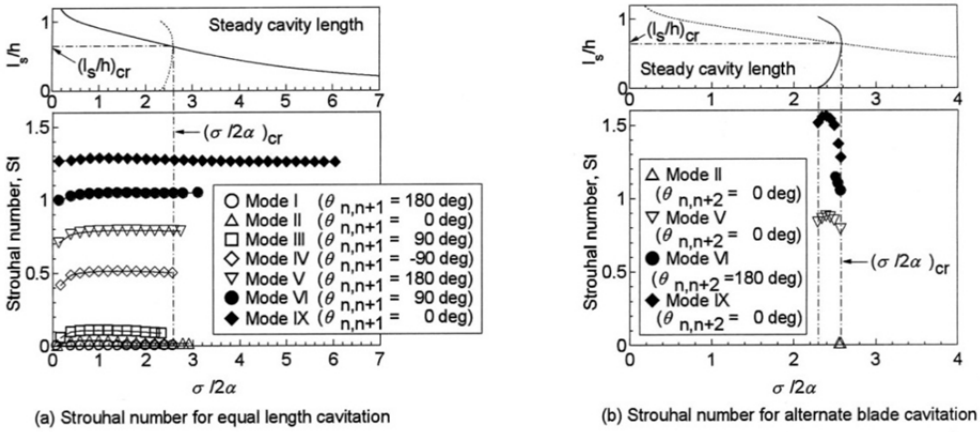

Figure 9. Results of 2-D stability analysis for a 4-bladed inducer.

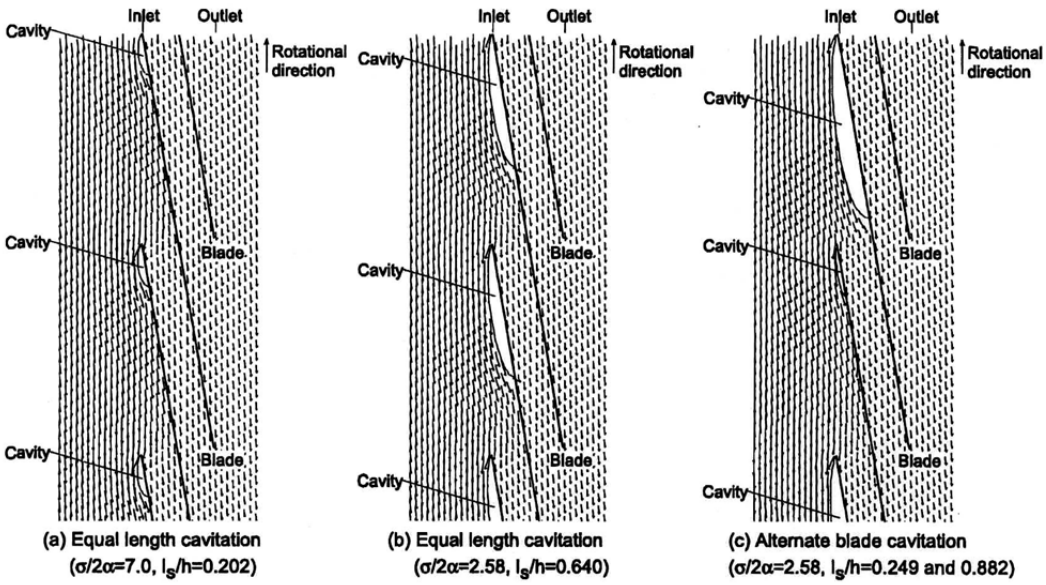

Figure 10. Alternate blade cavitation.

Figure 9 shows the results for a 4-bladed inducer. The steady cavity length l_s normalized with the blade spacing h is plotted against $\sigma/2\alpha$ in the upper part. The steady cavity length l_s/h generally increases with the decrease of $\sigma/2\alpha$. A solution corresponding to alternate blade cavitation starts to appear at $l_s/h=0.65$ in which the cavity length differs on alternate blades. The flows around equal and alternate blade cavitation are shown in Fig.10.

The Strouhal number $St=\omega_R l_S/2\pi U$ of amplifying modes with $\omega_I < 0$ is shown in the lower part of Fig.9. Figure 9(a) is for the equal length cavitation and (b) for alternate blade cavitation. In the figure, $\theta_{n,n+1}$shows the phase difference of the disturbance on adjacent blades. Mode I with $St = 0$ and $\theta_{n,n+1} = \pi$ shows that the equal length cavitation is statically unstable and transfers to alternate blade cavitation exponentially with time. Mode I does not exist for alternate blade cavitation showing that it is statically stable. Mode II, III, IV, V, VI show cavitation surge, normal rotating cavitation, rotating cavitation with counter rotation, alternate blade oscillation, and higher order surge mode oscillation, respectively. Thus, equal length cavitaty with longer than 65% of blade spacing is unstable to various modes of oscillation. In experiments, either cavitation surge or forward rotating cavitation occurs when the cavity at the tip becomes about 65% of the spacing. The higher order modes of surge and rotating cavitation sometimes occur but they are rare.

We consider about the cause of cavitation instabilities from the flow field shown in Fig.10. Figure 10 (b) shows that the flow near the cavity trailing edge is inclined towards the suction surface of the blade. This makes the angle of attack to the leading edge of the next blade smaller. Figure 10 (c) shows that the cavity on the next blade becomes smaller caused by the reduced angle of attack. The interaction of the local flow near the cavity trailing edge with the leading edge of the next blade is considered to be the cause of various cavitation instabilities since they start to occur when the cavity length becomes about 65% of the blade spacing.

5. Instabilities in pumping system:3-D flow analysis

In real flows, most of cavitation appears as bubble cloud cavitation near the tip as shown in Fig. 6. In order to understand cavitation instabilities under more realistic condition, a 3-D CFD was carried out under cavitating condition. The alternate blade cavitation was studied first, since a steady flow analysis is sufficient to simulate the flow.

Figure 11 shows the void fraction and the relative velocity at 98% radius of a 4-bladed inducer. Alternate blade cavitation occurs at $\sigma = 0.04$. With this calculation based on a bubbly flow model, the

velocity vector is not parallel to the cavity surface and the explanation used for the results of 2-D analysis cannot be applied. Then the disturbance velocity due to cavity was obtained by subtracting the non-cavitating flow vector from cavitating flow vector and is shown in Fig.12. This figure shows that outward velocity from the cavity can be seen near the leading edge where cavitation bubbles are growing, and that there exists a flow towards the cavity trailing edge where the bubbles are collapsing. The meridional flow shows that the radial component of the velocity is smaller than other components. At σ = 0.04 with alternate blade cavitation, the blade leading edge near the cavity trailing edge is exposed to axial velocity disturbance and the cavity on the blade is significantly small. Although the flow structure is different from those around 2-D blade surface cavity shown in Fig.10, the flow near the cavity trailing edge makes the incidence angle to the next blade in both cases.

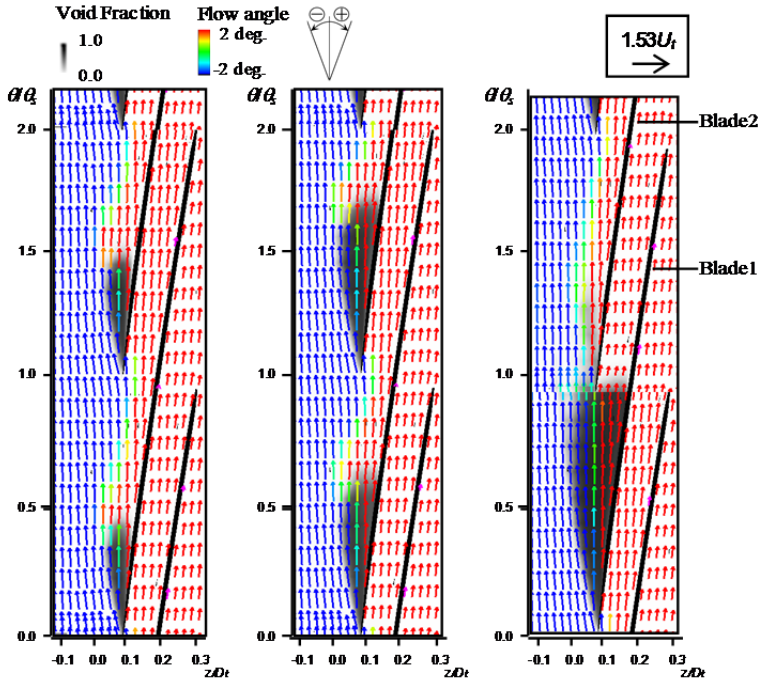

(a) σ=0.10 (b) σ=0.06 (c) σ=0.04

Figure 11. Void fraction and relative velocity field at 98% radius.

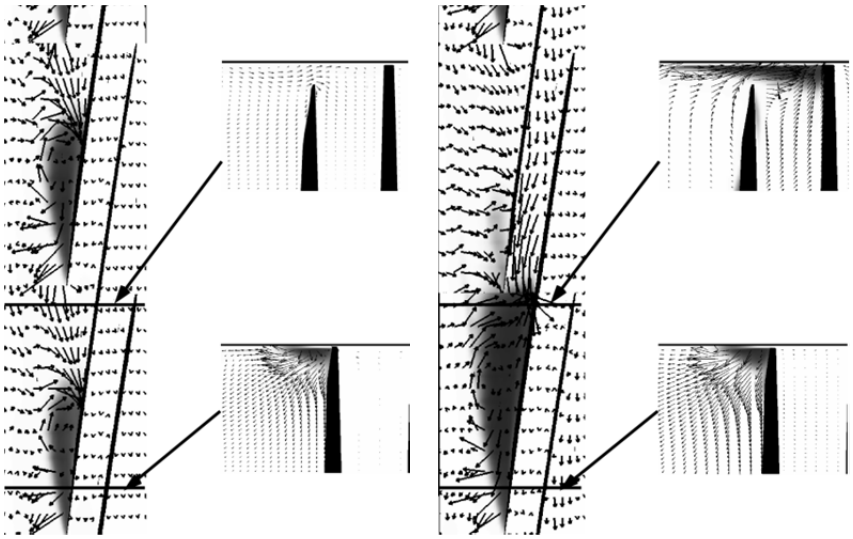

(a) σ=0.06 (b) σ=0.04

Figure 12. Void fraction and disturbance velocity around tip cavity.

Figure 13 shows the flow field and the void fraction in the 98% radius and the meridional plane AB under rotating cavitation, obtained by unsteady calculation. We can observe that the propagation occurs by the shrink of the cavity caused by the exposure of the leading edge to the higher axial velocity disturbance towards the trailing edge of the preceding blade.

These results by 2-D and 3-D flow analyses suggests that cavitation instabilities can be avoided by avoiding the interaction of the local flow near the cavity trailing edge with the next blade. This was confirmed by testing inducers designed to realize such situation[13],[14].

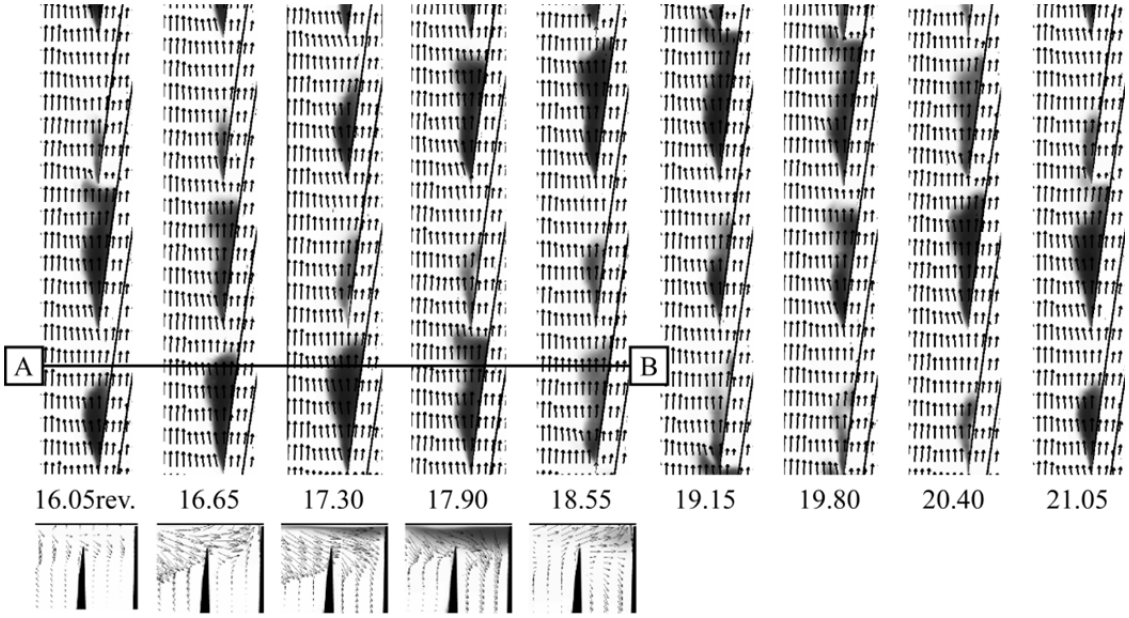

Figure 13. Void fraction and flow field under rotating cavitation.

6. Conclusion

It has been shown that the fundamental character of cavitation that the cavity volume increases if the pressure is decreased or the incidence angle is decreased causes various types of cavitation instabilities in hydraulic machinery. The cavity volume fluctuation affects the flow through continuity equation, not through the momentum equation. This makes it possible to build models of various levels and commercial CFD can give reasonable results. Although not treated in this manuscript, there are other types of cavitation instabilities called rotating choke[15],[17] and choked surge[16],[17], caused by the decrease of the pressure performance due to cavitation (choke). These are caused by the positive slope of the performance curve under cavitating condition and have similar characters to rotating stall and compressor surge.

Pumps and hydro turbines are requested to operate stably over a wide range of flow rates. Due to higher density of liquids, the fluid forces on hydraulic machines are much larger than those on pneumatic machines. This requires the complete understanding of instabilities. Although hydraulic machines are extensively used, they still have interesting problems to be solved as mentioned above. These are good test cases of modern experimental methods and CFD and the author wishes that young researchers are interested in the problems in this field.

References

[1] Jacob T and Prenant J E 1996 Francis Turbine Surge:Discussion and Data Base *18th IAHR Symposium hydraulic machinery and cavitation (Valencia, Spain, 16-19 Sep 1996)*
[2] Nishi M and Liu S H 2013 *International Journal of Fluid Machinery and Systems* **6**(1) 33-48
[3] Farhat M, Avellan F and Tsujimoto Y 2008 *Journal of Fluids Engineering* **130** 041106-1-6

[4] Chen C K, Nicolet C, Yonezawa K, Farhat M, Avellan F and Tsujimoto Y 2009 *International Journal of Fluid Machinery and Systems* **2**(3) 260-8
[5] Chen C K, Nicolet C, Yonezawa K, Farhat M, Avellan F and Tsujimoto Y 2010 *International Journal of Fluid Machinery and Systems* **3**(1) 80-90
[6] Chen C K, Nicolet C, Yonezawa K, Farhat M, Avellan F and Tsujimoto Y 2010 *International Journal of Fluid Machinery and Systems* **3**(1) 91-101
[7] Yonezawa K, Konishi D, Miyagawa K., Avellan F, Doerfler P and Tsujimoto Y 2012 *Int J Fluid Mach Syst* **5**(4) 152-60
[8] Kamijo K, Shimura T and Watanabe M 1980 *A Visual Observation of Cavitating Inducer Instability* (Japan: National Aerospace Laboratory) TR-598T
[9] Tsujimoto Y, Kamijo K and Brennen C E 2001 *Journal of Propulsion and Power* **17**(3) 636-43
[10] Watanabe S, Sato K, Tsujimoto Y and Kamijo K 1999 *Journal of Fluids Engineering* **121**(4) 834-40
[11] Horiguchi H, Watanabe S and Tsujimoto Y *Journal of Fluids Engineering* **122**(4) 798-805
[12] Kang D, Yonezawa K, Horiguchi H, Kawata Y and Tsujimoto Y 2009 *International Journal of Fluid Machinery and Systems* **2**(3) 206-14
[13] Kang D, Watanabe T, Yonezawa K, Horiguchi H, Kawata Y and Tsujimoto Y 2009 *International Journal of Fluid Machinery and Systems* **2**(4) 439-48
[14] Kang D, Arimoto Y, Yonezawa K, Horiguchi H, Kawata Y, Hah C and Tsujimoto Y 2010 *International Journal of Fluid Machinery and Systems* **3**(2) 137-49
[15] Semenov Y A, Fujii A and Tsujimoto Y 2004 *J. Fluids Eng.* 126(1) 87-93
[16] Watanabe T, Kang D, Cervone A, Kawata Y and Tsujimoto Y 2008 *International Journal of Fluid Machinery and Systems* **1**(1) 64-75
[17] Watanabe T, Sato H, Henmi Y, Horiguchi H, Kawata Y and Tsujimoto Y 2009 *International Journal of Fluid Machinery and Systems* **2**(3) 232-8